ANL-HEP-CP-76-37
CONF-760719--3

Inclusive Charged- and Neutral-Current Antineutrino-Proton Interactions at High Energy

By

M. Derrick, T. Dombeck, L. G. Hyman, K. Jaeger,
D. Lissauer, R. J. Miller, B. Musgrave, J. Phelan,
P. Schreiner, R. Singer,
S. J. Barish, A. Engler, G. Keyes, T. Kikuchi, R. W. Kraemer,
V. E. Barnes, D. D. Carmony, A. F. Garfinkel, and A. T. Laasanen

Prepared for

XVIII International Conference
on High Energy Physics
Tbilisi, USSR
July 15-21, 1976

U of C-AUA-USERDA

ARGONNE NATIONAL LABORATORY, ARGONNE, ILLINOIS

operated under contract W-31-109-Eng-38 for the
U. S. ENERGY RESEARCH AND DEVELOPMENT ADMINISTRATION

ANL-HEP-CP-76-37

Presented at the XVIII International Conference on
High Energy Physics, Tbilisi, USSR (July 15-21, 1976)

Inclusive Charged- and Neutral-Current Antineutrino-Proton Interactions at High Energy*

M. DERRICK, T. DOMBECK, L. G. HYMAN, K. JAEGER, D. LISSAUER+, R. J. MILLER, B. MUSGRAVE, J. PHELAN, P. SCHREINER, and R. SINGER

Argonne National Laboratory, Argonne, Illinois 60439

and

S. J. BARISH, A. ENGLER, G. KEYES, T. KIKUCHI, and R. W. KRAEMER

Carnegie-Mellon University, Pittsburgh, Pennsylvania 15213

and

V. E. BARNES, D. D. CARMONY, A. F. GARFINKEL, and A. T. LAASANEN

Purdue University, Lafayette, Indiana 47907

Results on antineutrino-proton interactions observed in the Fermilab 15-foot hydrogen bubble chamber are presented. The charged-current semi-inclusive distributions, as a function of X, Y, Q^2 and W, are compared with the predictions of the naive quark parton model. Within statistics, we observe no marked dependence of the Y distribution on E_ν. $R_{\bar{\nu}}$, the antineutrino neutral-current to charged-current cross section ratio is calculated, and results are presented as a function of R_ν.

---

*Work supported by the U. S. Energy Research and Development Administration.

+On leave of absence from Tel-Aviv University, Tel-Aviv, Israel.

I. Introduction

We present preliminary results on antineutrino-proton interactions observed in the Fermilab 15-foot hydrogen bubble chamber. The data were obtained in two separate exposures of 23,000 and 38,000 pictures, respectively. In the first (second) exposure, the antineutrino/neutrino beam was produced from a 300 GeV/c (400 GeV/c) extracted proton beam focused on an Al target. The average proton intensity per pulse was $\sim 6 \times 10^{12}$ (8×10^{12}). The produced negative and positive particles were focused and defocused, respectively, by one (two) magnetic "horn." The charged-current interaction rate was 1 event per 190 frames (1 event per 80 frames). All the data from the first exposure and ~60% of the data from the second exposure have been included in this analysis.

The film was scanned for all topologies with three or more prongs having a visible momentum in the forward hemisphere greater than 2 GeV/c. The scanning efficiency for these topologies is approximately 95%. (In a separate scan, the one-prong scanning efficiency is ~40%, and these events have not been included in the present analysis.) Tracks were reconstructed using a modified version of the ANL 12-foot chamber TVGP. After repeated measurements, the average event pass rate inside a 18.7 m^3 fiducial volume was 87%.

Interactions produced by the $\bar{\nu}/\nu$ beam can be grouped into the inclusive reactions

$$\bar{\nu} p \rightarrow \mu^{+} + \ldots . \qquad \bar{\nu}_{CC} \qquad (1)$$

$$\nu p \rightarrow \mu^{-} + \ldots . \qquad \nu_{CC} \qquad (2)$$

$$\bar{\nu} p \rightarrow \bar{\nu} + \ldots . \qquad \bar{\nu}_{NC} \qquad (3)$$

$$\nu p \rightarrow \nu + \ldots . \qquad \nu_{NC} \qquad (4)$$

Neutral Current

Note that antineutrino and neutrino neutral-current events (reactions 3 and 4) cannot be separated on an event-by-event basis.

II. Charged-Current Interactions

The correct identification of the muon track is crucial to the study of both charged-current and neutral-current events. In order to assign events to their respective inclusive channels, we use the following procedure:[1] Let R be the ratio of the momenta of the fastest to the second fastest charged track and $P_{\perp}^{m}$ be the largest momentum transverse to the beam direction of any track. If $R \geq 2$ the fastest track is assumed to be the muon; if $R \leq 2$ and $P_{\perp}^{m} \geq 1$ GeV/c that track is assumed to be the muon; if neither condition is satisfied, the event is classified as a neutral-current event. In addition, charged-current events were required to have a visible momentum greater than 5 GeV/c.

We have used the External Muon Identifier (EMI)[2] to check the reliability of our muon assignment and have found that the $\bar{\nu}_{CC}$ sample has less than 10% background. This is in agreement with the estimated contamination calculated using the number of tracks we have classified as μ^{+} by the above techniques which are observed to scatter in the bubble chamber. At

present, we do not use the EMI on an event-by-event assignment because of high "punch through" probability and because of low geometric acceptance of the EMI for high Y events.

The beam energy (E) for the events was calculated using a modified version of a technique proposed by A. Grant.[3] Using a Monte Carlo calculation, we have found the resulting resolutions in E, $X = Q^2/2M(E - E_\mu)$, $Y = (E - E_\mu)/E$, $Q^2 = (P_\nu - P_\mu)^2$ and W = hadronic mass to be ± 10%, ± 0.05, ± 0.07, ± 15% and ± 0.5 GeV, respectively. In Fig. 1, we show the calculated antineutrino/neutrino beam spectra[4] appropriate to the second exposure (P_p = 400 GeV/c). Where both spectra peak at ~ 15 GeV/c, the $\bar{\nu}$ flux falls off more rapidly than the ν flux, so that at $E_\nu > 120$ GeV, the neutrino flux is larger than the antineutrino flux. In Fig. 2, we show the energy distribution for the 332 $\bar{\nu}$p events selected to be charged-current events. The average energy/event is ~30 GeV.

The quark parton model (QPM) prediction for the differential cross section as a function of X and Y is given by the expression

$$\frac{d^2\sigma}{dXdY} = \frac{2G^2MEX}{\pi}\left[(1 - Y)^2\, u(X) + \bar{d}(X)\right] \qquad (5)$$

where u(X) and $\bar{d}(X)$ are the quark and antiquark distribution functions, respectively. Equation (5) can be rewritten in terms of W and Q^2 or V = XY and U = X/Y thus yielding predictions for the distribution in any of the variables X, Y, Q^2, W and V. In Fig. 3, we show the average value of Q^2 as a function of E_ν. A linear rise with energy is observed with a slope of (0.17 ± 0.011) GeV/c^2

in good agreement with the predictions of Barger and Phillips[5] and McElhaney and Tuan[6] of 0.19 and 0.17, respectively.

In Fig. 4, we show the Y distribution for all the data. The loss of events at low Y($Y \lesssim 0.1$) is due mainly to the loss of one-prong events which have not been included in this sample. The distribution has been corrected for events belonging to either neutral-current or neutrino charged-current events which were misidentified as antineutrino charged current, using the results of a Monte Carlo study. No correction was made for any biases in the Y distribution due to errors in identifying the μ^+ introduced by our muon selection criteria. (This effect is expected to be important only for $Y \geq 0.8$.) In Fig. 5 we show the X distritribution for events with $Y \geq 0.1$. The curves on both X and Y distributions are predictions of Barger and Phillips[5] and are in good agreement with the data. The dip observed for events with low X values is due in part to a loss of events at high Y.

In Figs. 6 and 7, we show the V = XY and W distributions for all events with $Y \geq 0.1$. The curves are predictions using the naive QPM,[5] and the agreement with the data is good.

In Fig. 8a, b we show the Y distributions for the two energy intervals $5 \leq E_{\bar{\nu}} \leq 30$ GeV and $E_{\bar{\nu}} > 30$ GeV, respectively. The Y distributions shown have been fitted to the form

$$dN/dY \propto \{(1 - Y + Y^2/2) - BY(1 - Y/2)\} \qquad (6)$$

for the range of $0.1 \leq Y \leq 0.8$. The parameter B is related to the relative antiquark content of the nucleon by $\bar{Q}/(Q + \bar{Q}) = \frac{1 - B}{2}$. The value B = 1 gives

a pure $(1 - Y)^2$ distribution, and the value B = -1 gives a flat distribution in Y. The resulting fits give B = 0.91 ± 0.08 and B = 0.82 ± 0.14 for $5 \leq E_{\bar{\nu}} < 30$ GeV and $E_{\bar{\nu}} > 30$ GeV, respectively. Assuming that there are no strong energy dependent corrections to the Y distribution, then there are no significant differences between the two distributions. In addition, within the statistics of this experiment, both distributions are consistent with $(1 - Y)^2$.

In Fig. 9a, b, c, we show the Y distribution for the different topologies; a strong correlation between Y and the multiplicity, n, is observed. The increase in the average value of Y with increasing n is probably a reflection of the correlation observed between Y and W, and W and n.

The properties of the hadronic system X^o in $\bar{\nu} p \rightarrow \mu^+ + X^o$ can be used to investigate the production mechanism involved in this reaction. Assuming the reaction proceeds via an exchange mechanism described in Fig. 10, it is interesting to compare the properties of the hadronic system X^o with those produced in other reactions, e.g., $e^- p \rightarrow e^- + X^+$. In Fig. 12, we show the invariant distribution of the Feynman variable, $X_F = P_{||}/2\sqrt{s}$, defined in the center of mass system of X^o, for the positive and negative pions. We note that both distributions exhibit the same feature showing a steeper slope in the proton fragmentation ($X_F = -1$) region than in the current, W, fragmentation region ($X_F = 1$). Both γp and $e^- p$ collisions show a similar effect. Using the QPM Sehgal has calculated the average π^- multiplicity in the current fragmentation region as a function of $Z = E_\pi/(E_\nu - E_\mu)$.[7] In Fig. 13, we show a comparison of the experimental $\langle z \cdot n_{\pi^-} \rangle$ distribution as a function of Z.

The curve shows the Sehgal calculation with absolute normalization. The agreement in the current fragmentation region (large Z) is excellent.

III. Neutral-Current Interactions

The existence of neutral-current events in both ν and $\bar{\nu}$ interactions has been observed previously.[8] In this experiment, we attempt to measure $R_{\bar{\nu}}$, the neutral-current to charged-current cross section ratio in hydrogen. Since neutral-current events cannot be assigned a unique beam energy, one can only calculate the average, $\langle R_{\bar{\nu}} \rangle$, integrated over our beam energy spectrum

$$R_{\bar{\nu}} = \frac{\int_{E_{min}}^{E_{max}} \frac{d\sigma}{dE}(\bar{\nu}p \rightarrow \bar{\nu} + \ldots)\, dE}{\int_{E_{min}}^{E_{max}} \frac{d\sigma}{dE}(\bar{\nu}p \rightarrow \mu^{+} + \ldots)\, dE} \quad . \tag{7}$$

In order to calculate $R_{\bar{\nu}}$ in this experiment, we first have to estimate the hadronic induced background in the neutral-current sample. In Fig. 14 we show the MM^2 distribution of the incident particle for all three-prong events assuming a final state of $pp\pi^-$ (i.e., $MM + p \rightarrow p + p + \pi^-$). A clear peak is seen near $MM^2 = M_n^2$ indicating a substantial contribution from neutron-induced reactions. After imposing a visible momentum cut of 3 GeV/c, most of the peak is removed. In Fig. 15a, b we show a scatter plot of ϕ vs. P_{VIS} (ϕ is the angle between the visible hadronic momentum vector and the beam direction and P_{VIS} is the visible momentum of the hadronic system) for $\bar{\nu}_{CC}$

and neutral-current events. Above 3 GeV/c, the angle ϕ for the $\bar{\nu}_{CC}$ system is bounded by 30^{o} while neutral-current candidates show a few events at high ϕ which are most probably neutron-induced background. The number of $np \rightarrow pp\pi^{-}$ events in the exposure was determined from 1C fits to this hypothesis together with the MM^{2} plot and by incorporating EMI information. The neutron background was determined from these events knowing the distribution in neutron momentum, and scaling by the known topological cross section ratio of $np \rightarrow 3$ prongs, $np \rightarrow 5$ prongs, etc. (as a function of neutron momentum) to the $np \rightarrow pp\pi^{-}$ cross section. The neutron background in the neutral-current sample of 127 events with $P_{VIS} \geq 3$ GeV/c was estimated to be 29 ± 10 events.

Knowing R_{ν}, the neutrino neutral-current to charged-current cross section ratio, the following relations can be solved for

$$N_1^E = N_1 \epsilon_{11} + N_2 \epsilon_{21} + N_3 \epsilon_{31} + N_4 \epsilon_{41}$$
$$N_2^E = N_1 \epsilon_{12} + N_2 \epsilon_{22} + N_3 \epsilon_{32} + N_4 \epsilon_{42}$$
$$N_{34}^E = N_1 \epsilon_{134} + N_2 \epsilon_{234} + N_3 \epsilon_{334} + N_4 \epsilon_{434}$$
$$0 = N_2 R_{\nu} - N_4$$

where the subscripts 1, 2, 3, 4 represent reactions (1), (2), (3), and (4), respectively. ϵ_{ij} is the probability that an event of reaction i will be classified as belonging to reaction j. N_i^E are experimental numbers of events found in each channel. The efficiencies ϵ_{ij} were calculated using a Monte Carlo program. The events were generaged with X, Y distributions predicted by the QPM with quark density functions given by Barger and Phillips[5] (1974). The

coefficients c_{ij} were found to be insensitive to θ_w, the Weinberg angle. We have used $\sin^2\theta_w = 0.35$ for our final calculation. In Fig. 16 we show our results for $R_{\bar{\nu}}$ as a function of R_ν. The error reflects both statistical and estimated systematic uncertainty. Note that the QPM predicts different ratios of $R_{\bar{\nu}}$ on protons and neutrons; thus one does not expect to make direct comparison of this experiment with experiments on complex nuclei.

References

1. M. Derrick et al., Phys. Rev. Letters 36, 936 (1976).

2. R. J. Cence et al., (University of Hawaii-Lawrence Berkeley Laboratory Collaboration), to be published.

3. A. Grant, CERN Report No. CERN/D. Ph. II/Phys. 75-7 (unpublished); S. J. Barish et al., Carnegie-Mellon University Report No. C00-3066-61 (unpublished).

4. We have calculated the flux spectrum using the pion and kaon yields measured by the Harvard-Pennsylvania-Wisconsin- Fermilab collaboration at Fermilab (R. Stefanski, private communication).

5. V. Barger and R. Phillips, Nucl. Phys. B73, 269 (1974).

6. R. McElhaney and S. F. Tuan, Nucl. Phys. B72, 487 (1974).

7. L. Sehgal, Nucl. Phys. B90, 471 (1975).

8. F. Hasert et al., Phys. Letters 46B, 138 (1973); B. Aubert et al.,

Phys. Rev. Letters 32, 800 (1974); S. J. Barish et al., Phys. Rev. Letters 33, 448 (1974).

Figure Captions

Fig. 1 Antineutrino/neutrino beam flux distribution for 400 GeV/c incident protons.

Fig. 2 Beam energy distribution for $\bar{\nu}_{CC}$ events.

Fig. 3 $\langle Q^2 \rangle$ vs. $E_{\bar{\nu}}$ for $\bar{\nu}_{CC}$ events.

Fig. 4 dN/dY distribution for $\bar{\nu}_{CC}$ events. The curve is $(1 - Y)^2$ normalized to number of events for $Y > 0.1$.

Fig. 5 dN/dX distribution for $\bar{\nu}_{CC}$ events. The curves are predictions using the QPM from Refs. (5) and (6) for $Y > 0.1$.

Fig. 6 dN/dV distribution for $\bar{\nu}_{CC}$ events with $Y > 0.1$. Curves are predictions of the QPM.

Fig. 7 dN/dW distribution for $\bar{\nu}_{CC}$ events with $Y > 0.1$.

Fig. 8 dN/dY distribution for $\bar{\nu}_{CC}$ events with (a) $5 \leq E_{\bar{\nu}} \leq 30$ GeV and (b) $E_{\bar{\nu}} \geq 30$ GeV. The curves are the results of the best fit to Eq. (6).

Fig. 9 dN/dY distributions for $\bar{\nu}_{CC}$ events with (a) 3-prong topologies, (b) 5-prong topologies, and (c) 7-11 prong topologies.

Fig. 10 Exchange diagram describing production of $\bar{\nu} p \rightarrow \mu^+ + X^0$.

Fig. 11 X_F invariant distribution for π^+ tracks in $\bar{\nu}_{CC}$ events.

Fig. 12 X_F invariant distribution for π^- tracks in $\bar{\nu}_{CC}$ events.

Fig. 13 $(Z/\sigma_T)\frac{d\sigma}{dZ}(\pi^-)$ for π^- tracks in the $\bar{\nu}_{CC}$ events. The curve is an absolute prediction of Sehgal using the QPM.

Fig. 14 MM^2 distribution for all three-prong events assuming the reaction $MM+p \rightarrow pp\pi^-$. The shaded region contains events with visible momentum greater than 3 GeV/c.

Fig. 15 Scatter plot of ϕ vs. P_{VIS} for the hadronic system of (a) $\bar{\nu}_{CC}$ events and (b) neutral-current candidates.

Fig. 16 Results of $R_{\bar{\nu}p}$ vs. $R_{\nu p}$ with predictions of the Weinberg-Salam model, using quark distribution functions given by Barger and Phillips (1974).

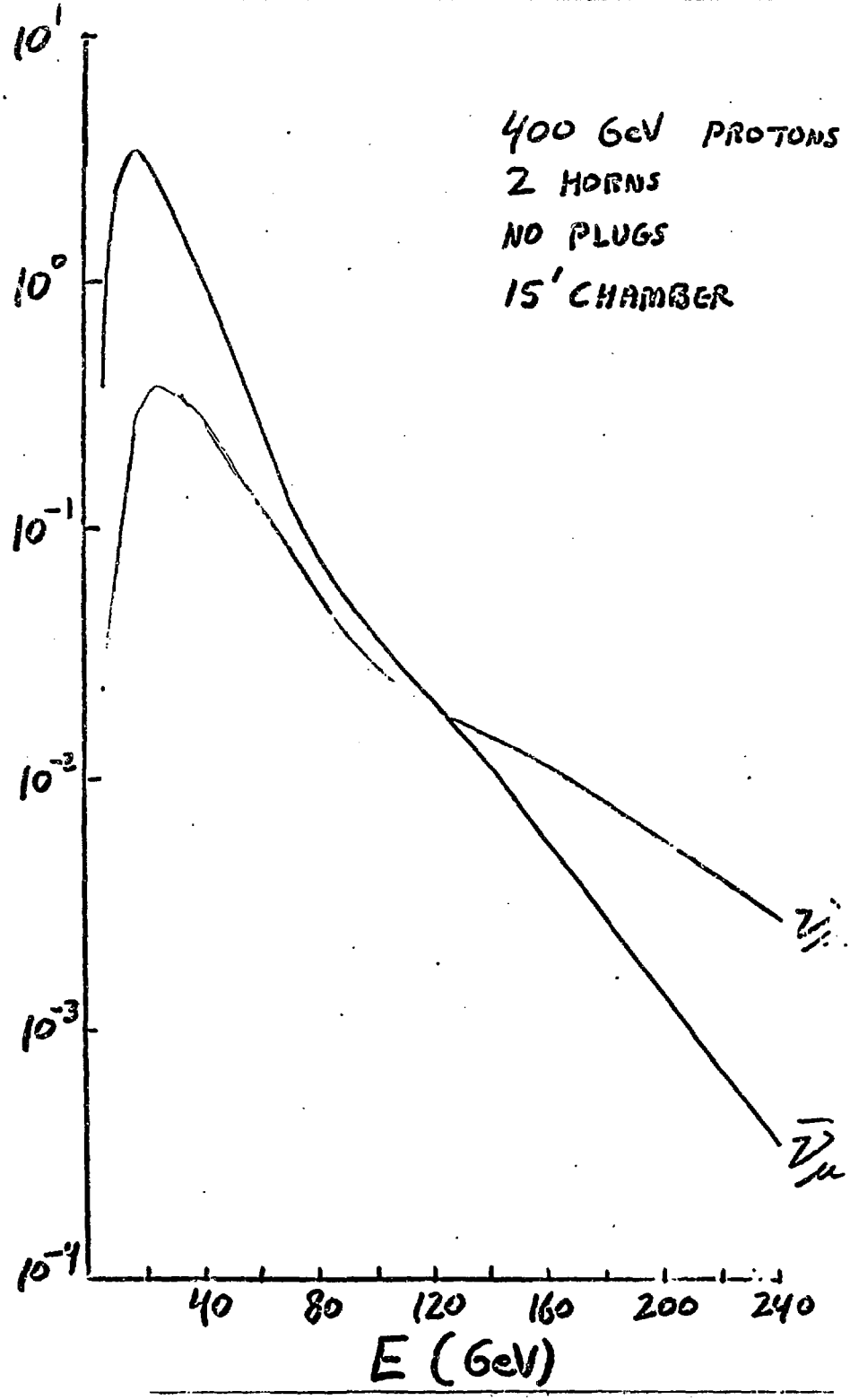
400 GeV PROTONS
2 HORNS
NO PLUGS
15' CHAMBER
10^1
10^0
10^{-1}
10^{-2}
10^{-3}
10^{-4}
ν_μ
$\bar{\nu}_\mu$
40
80
120
160
200
240
E (GeV)

Fig 1

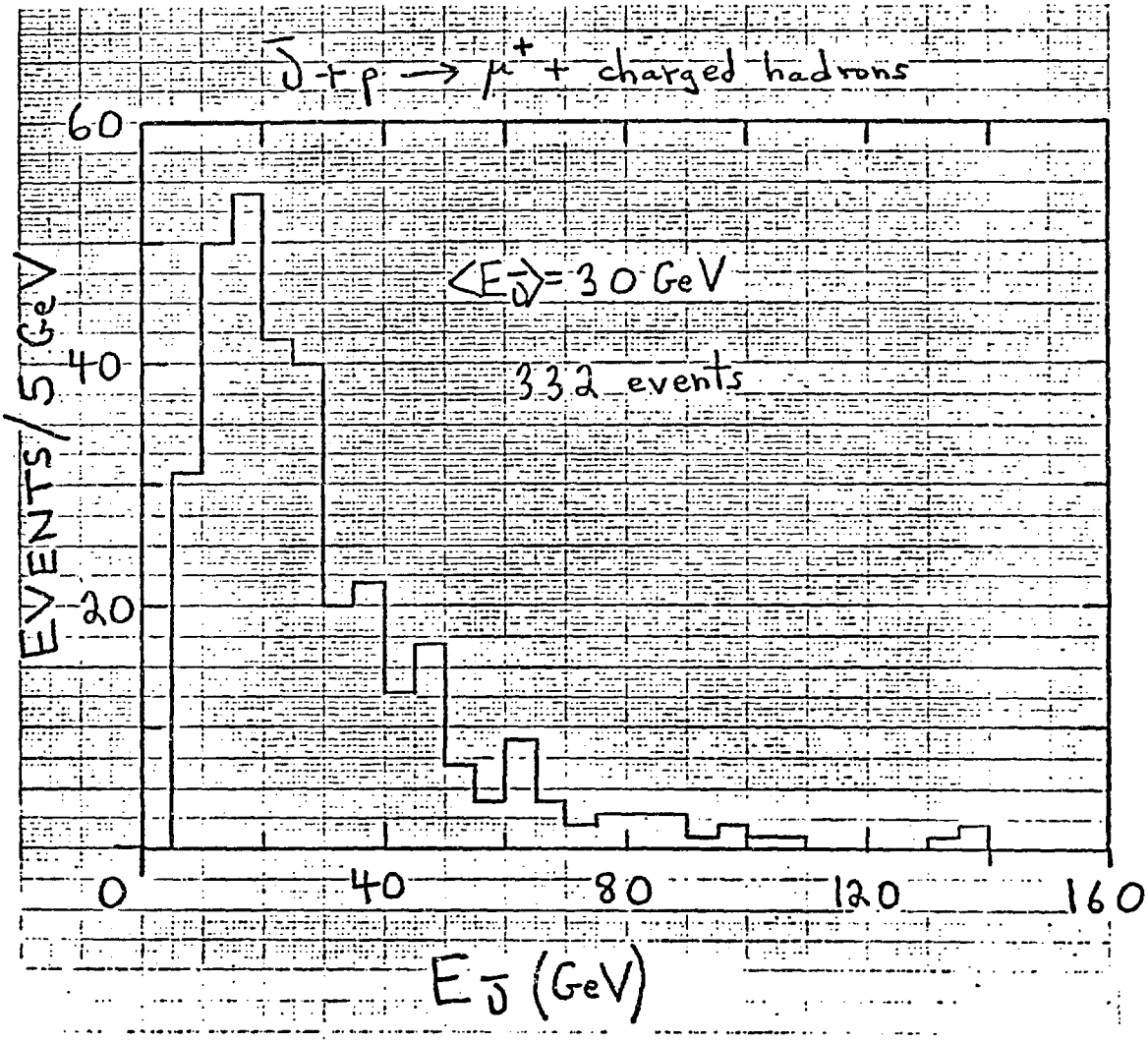
$\bar{\nu}_\mu + p \rightarrow \mu^+ +$ charged hadrons
$\langle E_{\bar{\nu}} \rangle = 30$ GeV
332 events
EVENTS / 5 GeV
60
40
20
0
40
80
120
160
$E_{\bar{\nu}}$ (GeV)

Fig 2

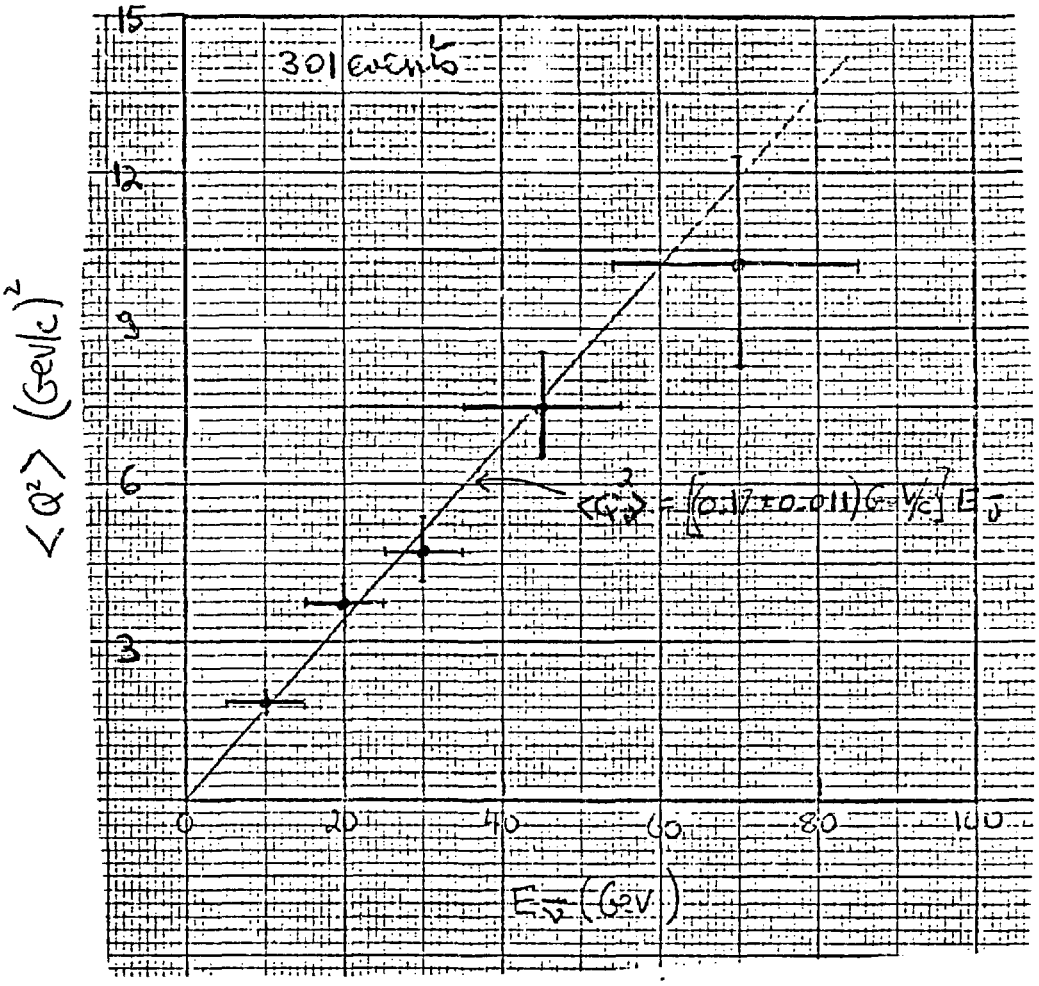
301 events
15
12
9
6
3
0
20
40
60
80
100
$\langle Q^2 \rangle$ (GeV/c)^2
E_ν (GeV)
$\langle Q^2 \rangle = [(0.17 \pm 0.01)\,\mathrm{GeV/c}]\,E_\nu$

Fig 3.

Fig 4.

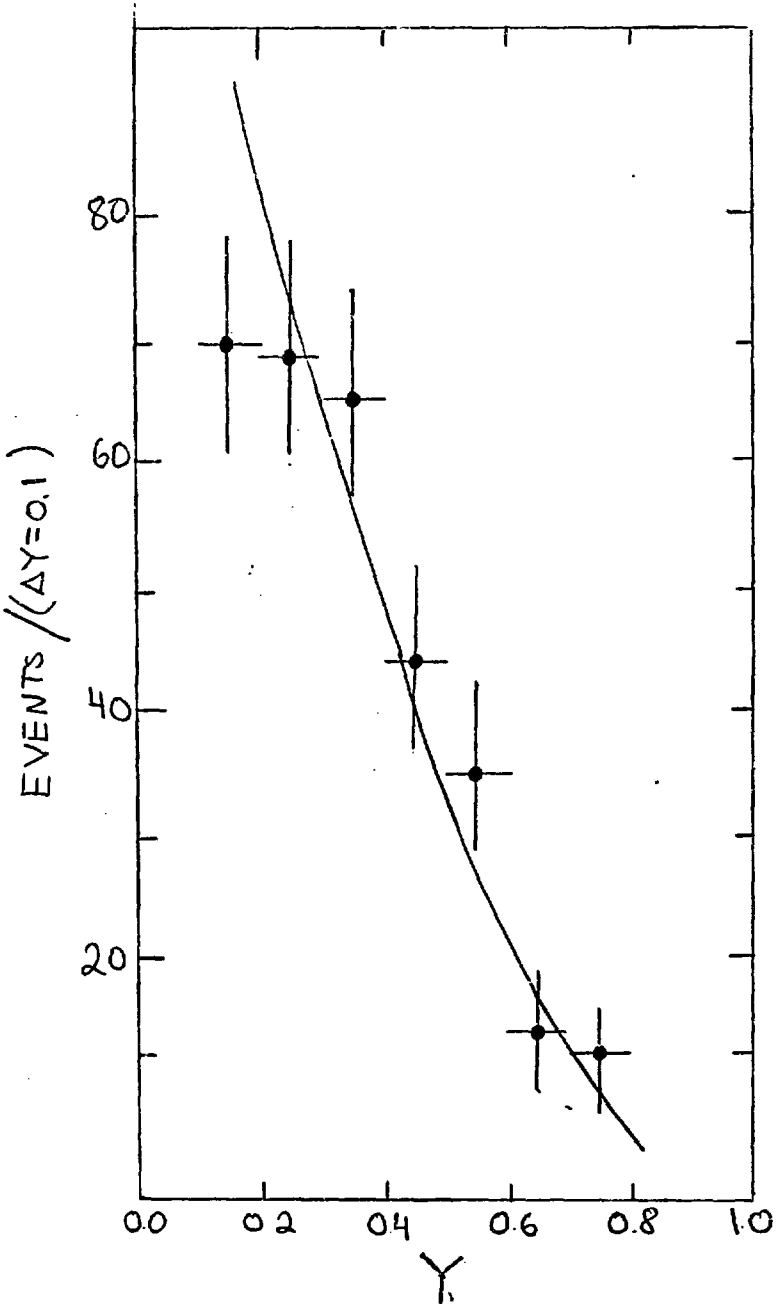

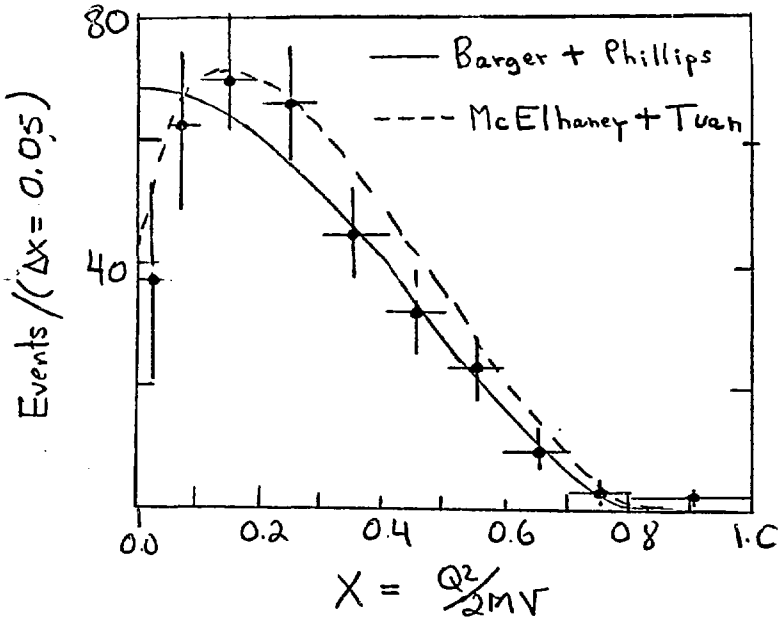
80
40
Events /(Δx = 0.05)
Barger + Phillips
McElhaney + Tuan
0.0
0.2
0.4
0.6
0.8
1.0
X = Q²/2Mν

Fig 5.

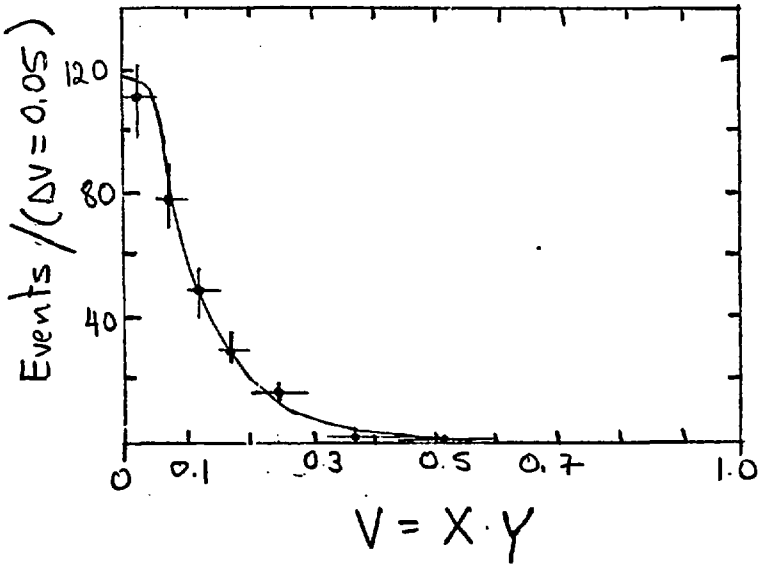
120
80
40
Events /(ΔV = 0.05)
0
0.1
0.3
0.5
0.7
1.0
V = X · Y

Fig 6.

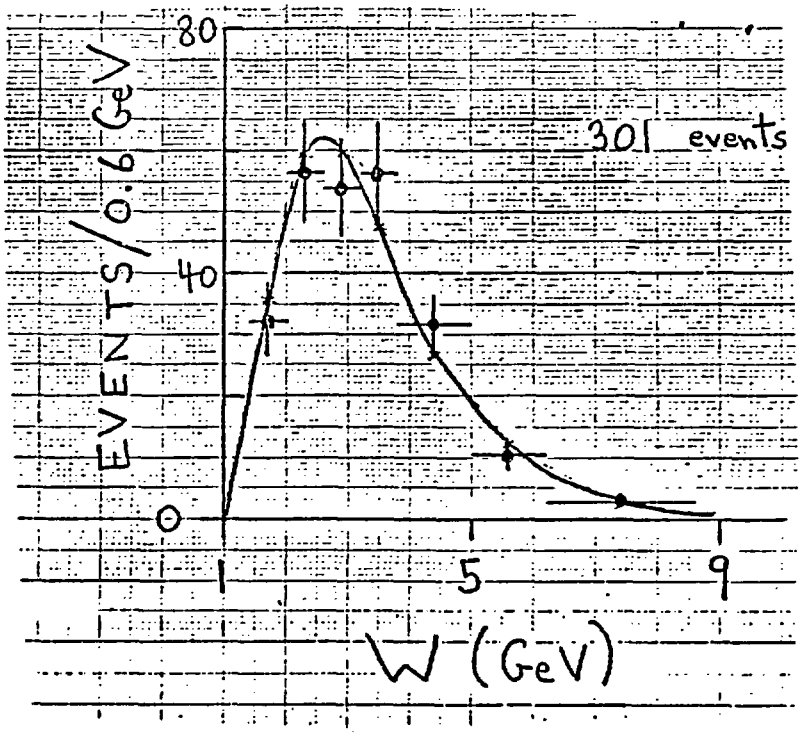

Fig 7

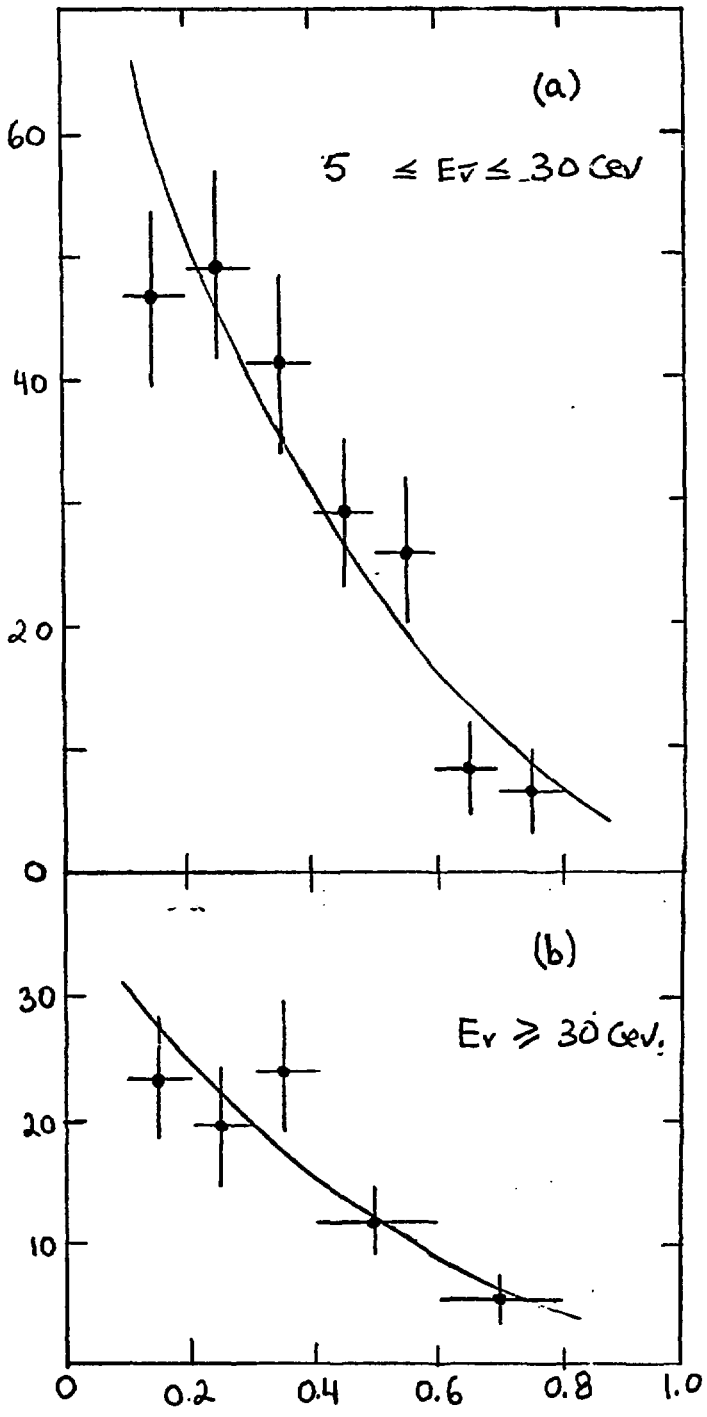

Fig 8.

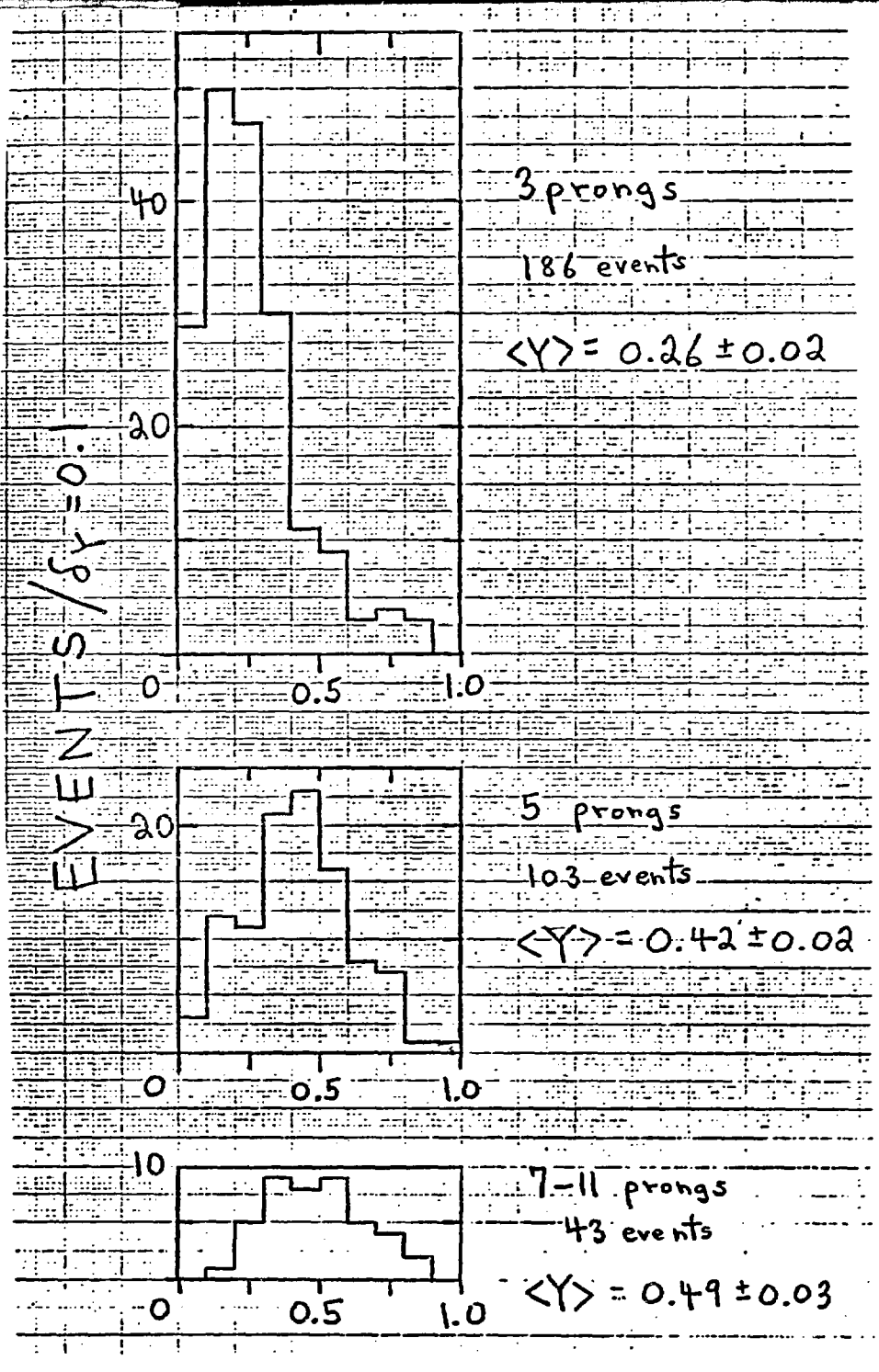
3 prongs
186 events
<Y> = 0.26 ± 0.02
40
20
0
0.5
1.0
5 prongs
103 events
<Y> = 0.42 ± 0.02
20
0
0.5
1.0
7-11 prongs
43 events
<Y> = 0.49 ± 0.03
10
0
0.5
1.0
dN/dY = 0.5 (1/σ dσ/dY)

Fig 9.

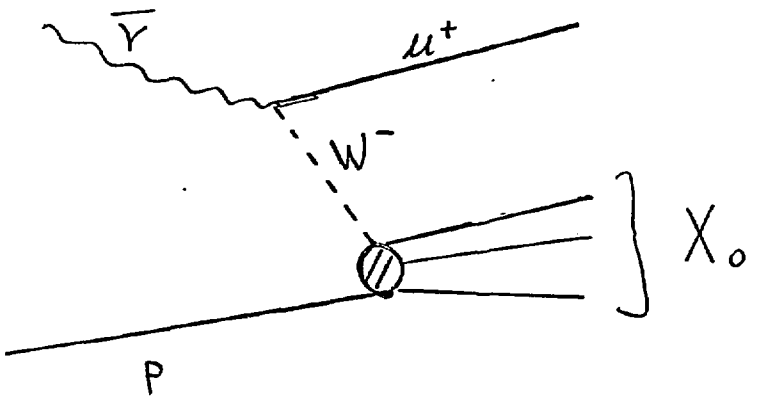

Fig 10.

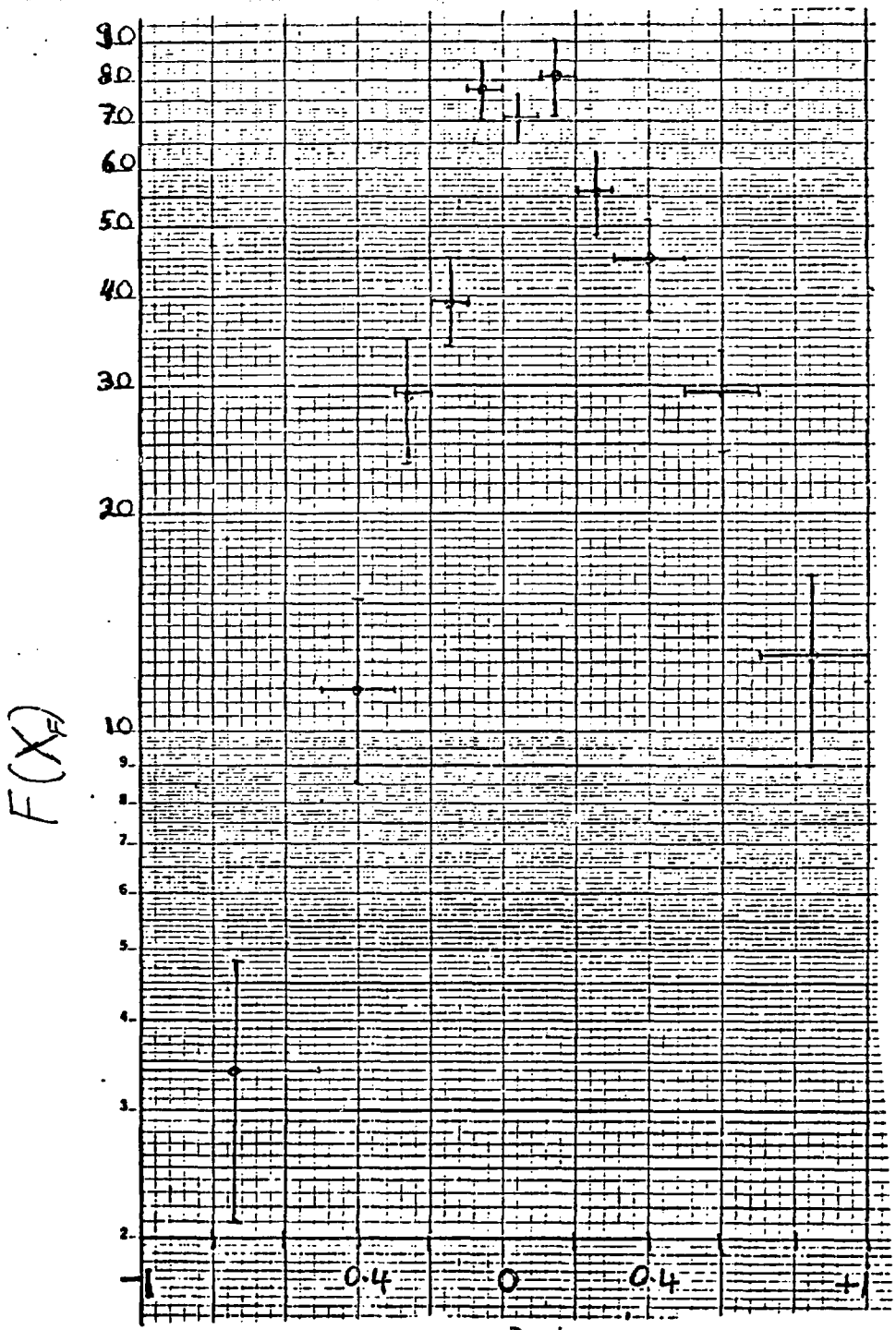

Fig 11

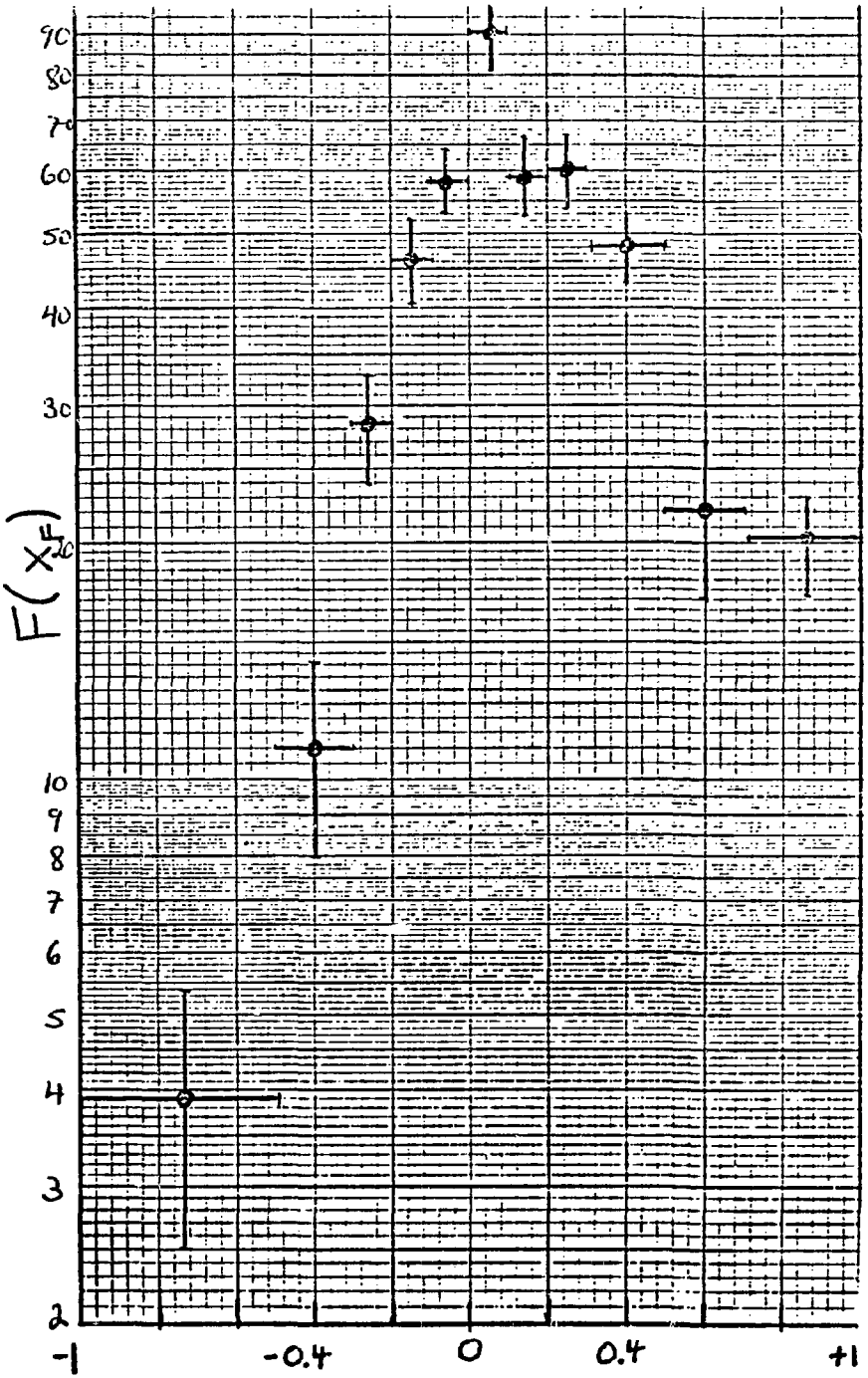

$$X_F = \frac{2 p_{11}}{\sqrt{s}}$$

Fig. 12

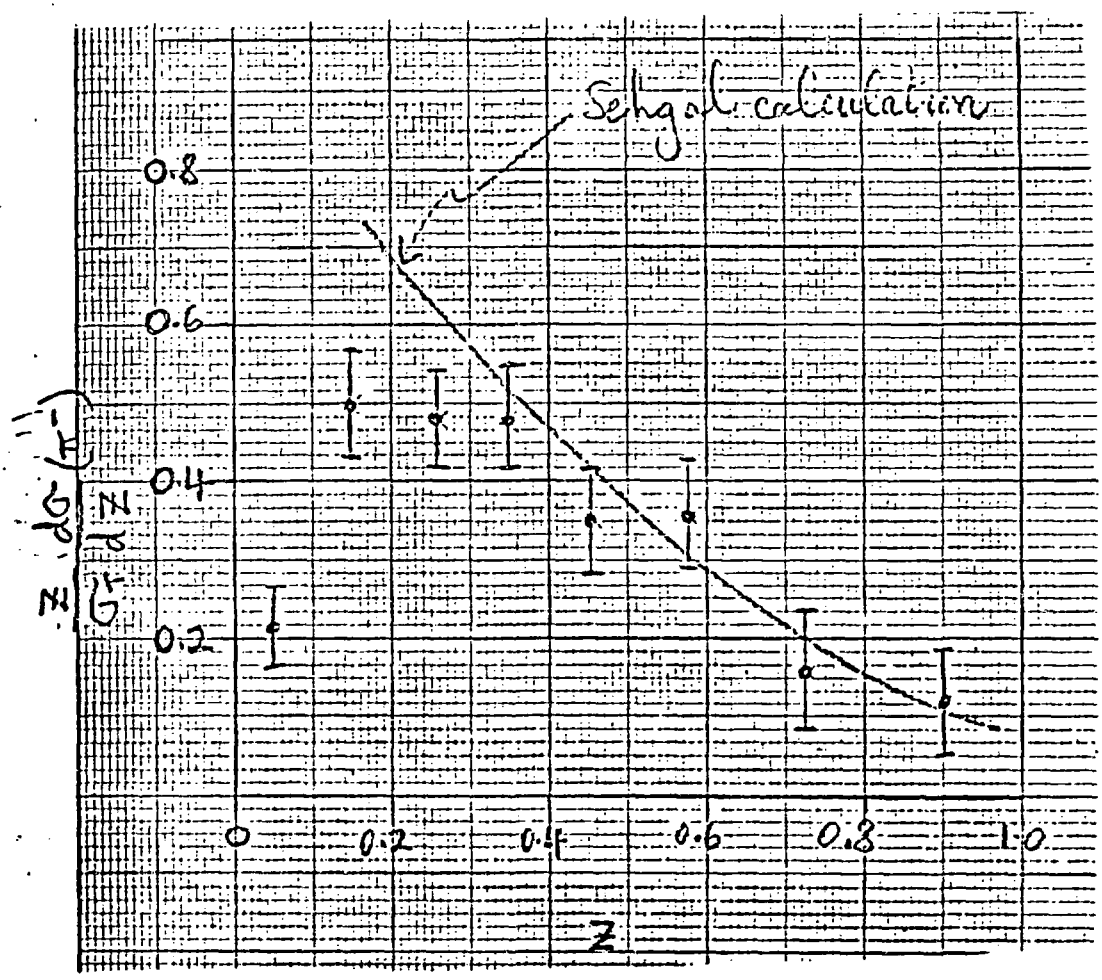

Fig 13.

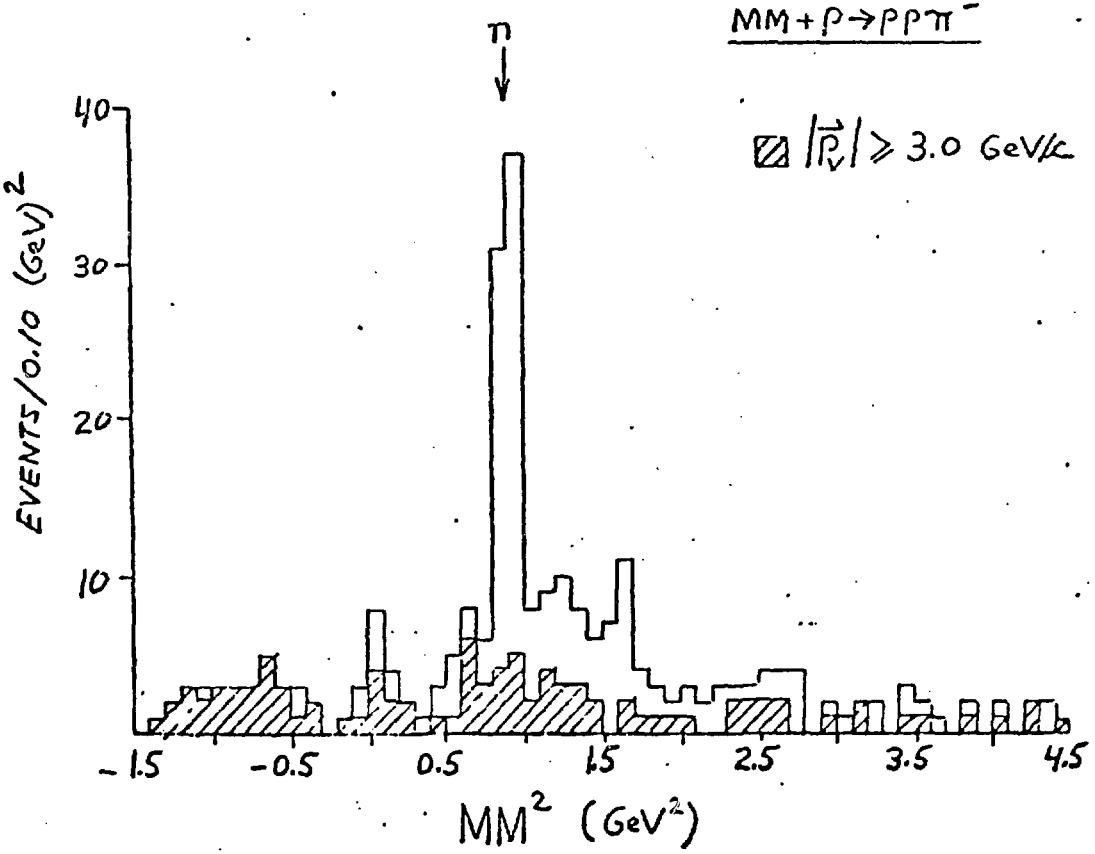
MM + p → p p π⁻
η
|p⃗_v| ≥ 3.0 GeV/c
EVENTS/0.10 (GeV)²
40
30
20
10
-1.5
-0.5
0.5
1.5
2.5
3.5
4.5
MM² (GeV²)

Fig 14.

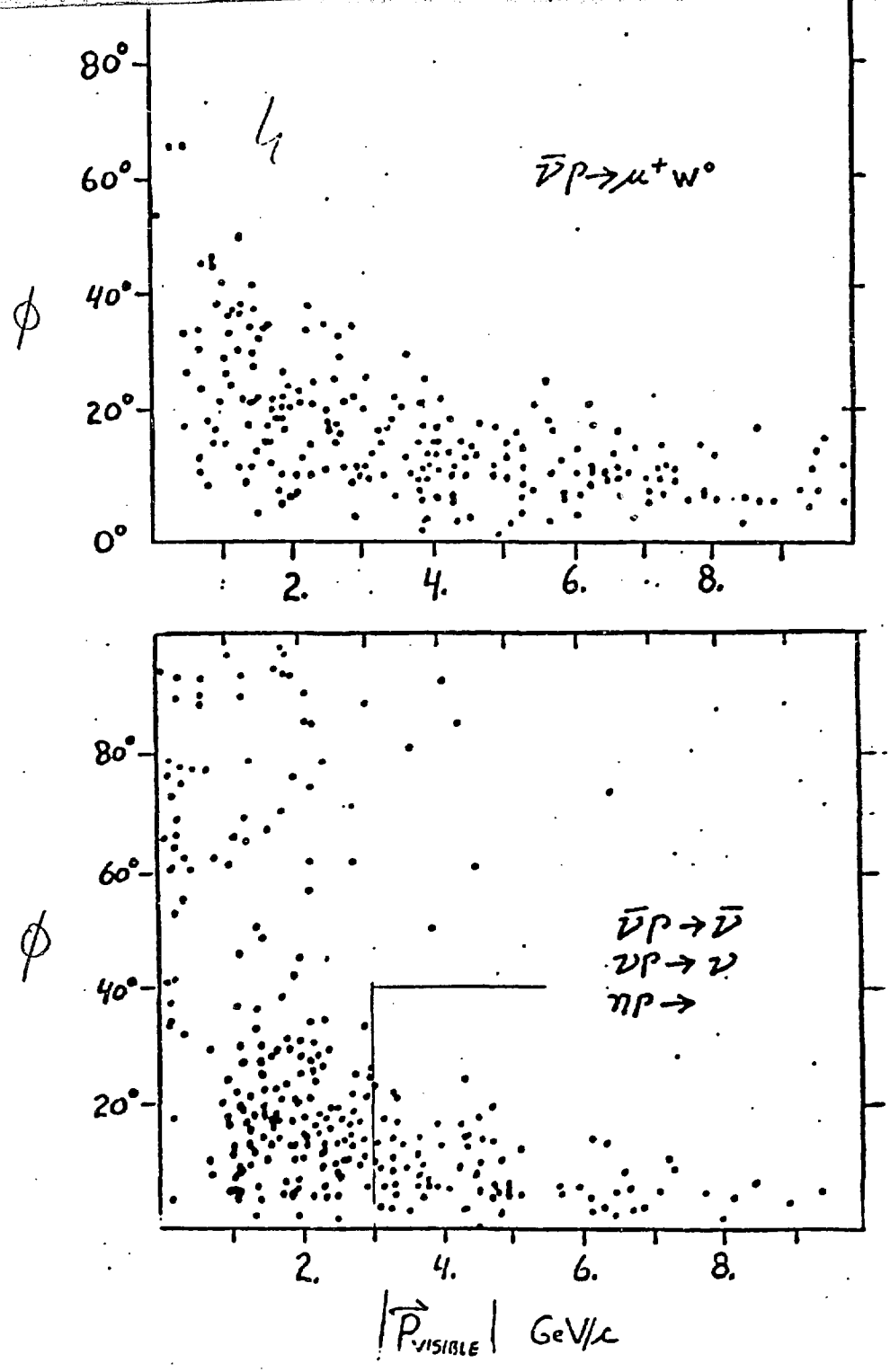
4
$\bar{\nu}p \to \mu^+ w^\circ$
80°
60°
40°
20°
0°
ϕ
2.
4.
6.
8.
$\bar{\nu}p \to \bar{\nu}$
$\nu p \to \nu$
$np \to$
$|\vec{P}_{VISIBLE}|$ GeV/c

Fig 15.

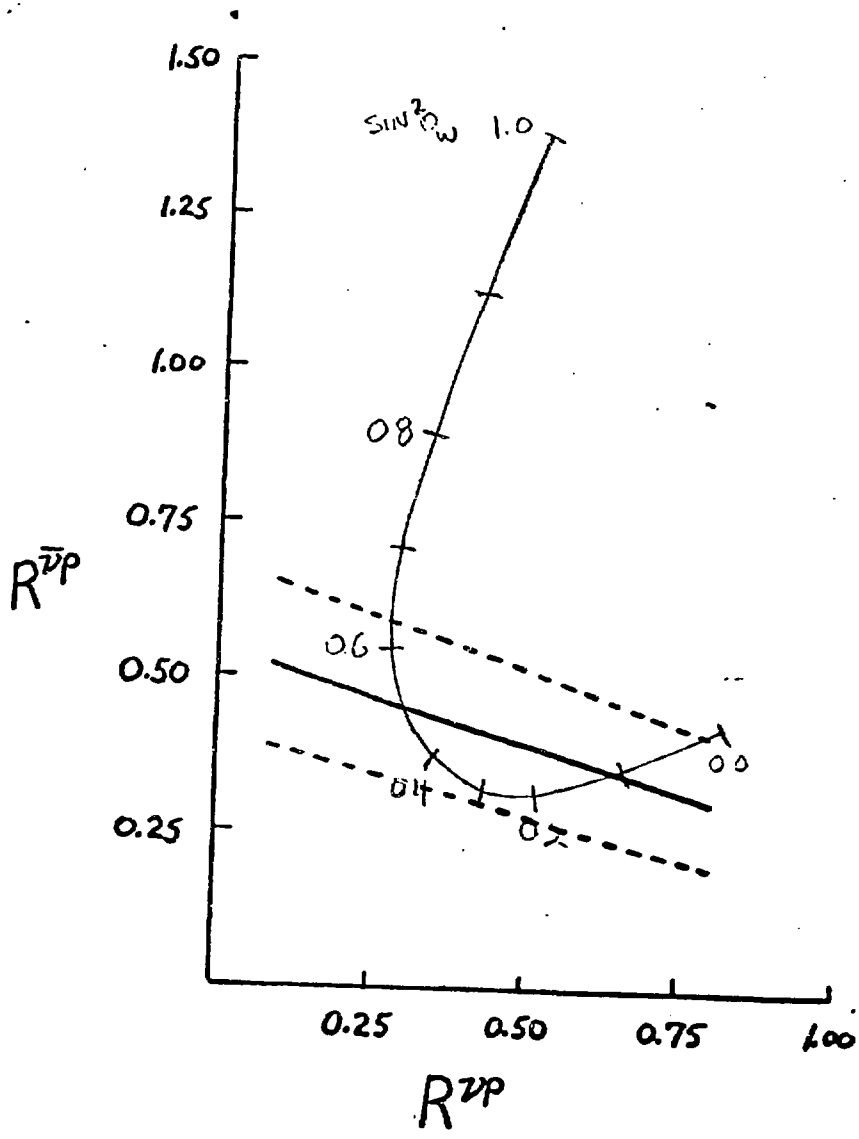
1.50
1.25
1.00
0.75
0.50
0.25
$R^{\bar{\nu}p}$
$\sin^2\theta_W$ 1.0
0.8
0.6
0.4
0.2
0.0
0.25
0.50
0.75
1.00
$R^{\nu p}$

Fig 16